Ain Shams Engineering Journal (2016) xxx, xxx–xxx

Ain Shams University

Ain Shams Engineering Journal

www.elsevier.com/locate/asej
www.sciencedirect.com

ENGINEERING PHYSICS AND MATHEMATICS

# Thermal radiation energy due to SWCNTs on MHD nanofluid flow in the presence of seawater/water: Lie group transformation

**R. Kandasamy** [a,*], **Vibhu Vignesh** [b], **Ashwin Kumar** [b], **Sulaiman Haji Hasan** [b], **Norasikin Mat Isa** [b]

[a] *Research Centre for Computational Fluid Dynamics, FSTPi, Universiti Tun Hussein Onn Malaysia, Malaysia*
[b] *Faculty of Manufacturing and Mechanical Engineering, Universiti Tun Hussein Onn Malaysia, Malaysia*

Received 4 December 2015; revised 2 April 2016; accepted 29 April 2016

**KEYWORDS**

Water and seawater based SWCNTs;
Porous wedge sheet;
Lie group analysis;
Thermal energy radiation

**Abstract** An investigation of the boundary layer nanofluids flow over a porous wedge in the presence of uniform transverse magnetic field and thermal radiation energy has been analyzed. Water and seawater based nanofluid containing copper, aluminum oxide and Single Walled Carbon nanotubes (SWCNTs) is taken into consideration. The governing equations in terms of ODEs are solved using fourth–fifth order Runge–Kutta–Fehlberg method with shooting technique. Approximate solution of temperature, velocity, the rate of heat transfer and the shear stress at the wedge are illustrated graphically for several values of the pertinent parameters. Thermal conductivity enhancements of water and seawater in the presence of single-walled carbon nanotubes (SWCNTs) are presented. The thermal boundary layer of SWCNTs–water is compared to SWCNTs–seawater on absorbing the incident thermal energy radiation and transmitting it to the nanofluid by convection. Momentum and thermal boundary layer thickness for SWCNTs–seawater is stronger than SWCNTs–water with increase of the radiation parameter because of low thermal conductivity of seawater. The rate of heat transfer of Cu–seawater is significantly stronger than all the other mixtures in the flow regime because of the combined effects of density of copper and seawater.


## 1. Introduction

Thermal conductivities of nanofluids containing SWCNTs dispersed in the presence seawater are improved significantly compared to freshwater. The study of the CNT filled with fluids is of significant interest and is a challenging topic for investigators. The interesting electrical and physical properties of both the single-walled and multi-walled CNTs have been seen to be a rich source of new physics [1–12]. Carbon

* Corresponding author. Tel.: +60 7 453 7416; fax: +60 7 453 6051.
E-mail address: future990@gmail.com (R. Kandasamy).
Peer review under responsibility of Ain Shams University.

Production and hosting by Elsevier

http://dx.doi.org/10.1016/j.asej.2016.04.022

**Nomenclature**

| | |
|---|---|
| $B_0$ | magnetic flux density, kg $s^{-2}$ $A^{-1}$ |
| $C_T$ | temperature ratio, K |
| $c_p$ | specific heat at constant pressure, J $kg^{-1}$ $K^{-1}$ |
| $g$ | acceleration due to gravity, m $s^{-2}$ |
| $Gr$ | Grashof number, – |
| $k_1$ | rate of chemical reaction, mol $m^{-1}$ $s^{-1}$ |
| $k^*$ | mass absorption coefficient, $m^{-1}$ |
| $K$ | permeability of the porous medium, $m^2$ |
| $k_f$ | thermal conductivity of the base fluid, kg m $s^{-3}$ $K^{-1}$ |
| $k_s$ | thermal conductivity of the nanoparticle, kg m $s^{-3}$ $K^{-1}$ |
| $k_{nf}$ | effective thermal conductivity of the nanofluid, kg m $s^{-3}$ $K^{-1}$ |
| $M$ | magnetic parameter, – |
| $N$ | thermal radiation parameter, – |
| $Pr$ | Prandtl number, – |
| $Re$ | Reynolds number, – |
| $q''_{rad}$ | incident radiation flux of intensity, kg $m^{-1}$ $s^{-3}$ $K^{-1}$ |
| $Q_0$ | rate of source/sink, kg $m^{-2}$ |
| $t$ | time, s |
| $T$ | temperature of the fluid, K |
| $T_w$ | temperature of the wall, K |
| $T_\infty$ | temperature of the fluid far away from the wall, K |
| $x, y$ | streamwise coordinate and cross-stream coordinate, m |
| $u, v$ | velocity components in $x$ and $y$ direction, m $s^{-1}$ |
| $U(x)$ | flow velocity of the fluid away from the wedge, m $s^{-1}$ |
| $V_0$ | velocity of suction/injection, m $s^{-1}$ |

*Greek symbols*

| | |
|---|---|
| $\alpha_{nf}$ | thermal diffusivity of the nanofluid, $m^2$ $s^{-1}$ |
| $\beta_f$ | thermal expansion coefficients of the base fluid, $K^{-1}$ |
| $\rho_f$ | density of the base fluid, kg $m^{-3}$ |
| $\rho_s$ | density of the nanoparticle, kg $m^{-3}$ |
| $\rho_{nf}$ | effective density of the nanofluid, kg $m^{-3}$ |
| $(\rho c_p)_{nf}$ | heat capacitance of the nanofluid, J $m^{-3}$ $K^{-1}$ |
| $(\rho\beta)_{nf}$ | volumetric coefficient of thermal expansion of nanofluid, $K^{-1}$ |
| $\sigma$ | electrical conductivity, $\Omega^{-1}$ $m^{-1}$ |
| $\sigma_1$ | Stefan–Boltzmann constant, kg $s^{-3}$ $K^{-4}$ |
| $\mu_f$ | dynamic viscosity of the base fluid, kg $m^{-1}$ $s^{-1}$ |
| $\mu_{nf}$ | effective dynamic viscosity of the nanofluid, kg $m^{-1}$ $s^{-1}$ |
| $v_{nf}$ | dynamic viscosity of the nanofluid, $m^2$ $s^{-1}$ |
| $\delta$ | time-dependent length scale, s |
| $\delta_1$ | heat source/sink parameter – |
| $\lambda$ | porous parameter, – |
| $\Omega$ | resistance, kg $m^2$ $s^{-3}$ $A^{-2}$ |
| $\xi$ | distance along the wedge, m |
| $\zeta$ | nanoparticle volume fraction, – |
| $\psi$ | dimensionless stream function, – |
| $\eta$ | similarity variable, – |
| $f$ | dimensionless stream function, – |
| $\theta$ | dimensionless stream function, – |

nanotubes can be visualized as a sheet of graphite that has been reformed into a tube, with diameters ranging roughly from 1 to 100 nm and lengths up to millimeters. The characteristic of CNTs to have metallic as well as semiconductor behavior depends on the diameter of the tubes. Due to thermal conductivity of energy transfer fluids used in power generation, microelectronics heating or cooling, chemical production and transportation and many other applications, it is compulsory to enhance thermal conductivity of these fluids to improve heat transfer. Because of mechanical properties, chemical and thermal stability, and hollow geometry, the carbon nanotube (CNT) promises many new applications in nanobiological devices and nanomechanical systems such as fluid storage, fluid transport, and drug delivery [13–17]. The nonlocal beam models have been adopted for different analyses of carbon nanotubes because it takes the nanoscale effect into account [18–21].

Nanofluids consist of nanometer-sized particles with significantly strong thermal conductivity dispersed in a common base fluid such as water or seawater. Due to their efficient thermal conductivity compared to base fluids and their performance in energy devices, nanofluids are interesting candidates for heat transfer enhancement [22–26]. Hence, the water based single walled carbon nanotubes (SWCNTs-water) for heat transfer enhancement in coaxial tube exchange due to thermal radiation under laminar flow regime are investigated numerically. These nanofluids appear to have a very strong thermal conductivity and may be able to meet the rising demand as an efficient heat transfer agent [27–29]. Several studies have been observed on the heat transfer enhancement of nanofluids flowing through a tube under the laminar regime. It is stated that the experimental convective heat transfer coefficients of nanofluids varied to increase the flow velocity and volume fraction. SWCNTs have unique electronic and mechanical properties which can be utilized in numerous applications [30–36]. The characteristics of seawater correspond to those of water in general, because of their common mechanical and physical properties, for example, the molecular structure of seawater, like that of freshwater, helps the formation of bonds among molecules. Some of the distinctive characteristics of seawater are attributable to its salt content. The viscosity (i.e., internal resistance to flow) of seawater, for example, is stronger than that of freshwater because of its higher salinity. The density of seawater is higher for the same reason. Seawater's freezing point is lower than that of freshwater, and its boiling point is stronger [37–40]. Recently, Rizwan et al. [41] investigated the convective heat transfer in MHD slip flow past a stretching surface in the presence of carbon nanotubes. In the present article, heat transfer of SWCNTs on MHD unsteady flow over a porous wedge in the presence of seawater and freshwater is analyzed.

The aim of the present work was to investigate the boundary layer flow of water and seawater based nanoparticles past a porous wedge in the presence of uniform transverse magnetic

Please cite this article in press as: Kandasamy R et al., Thermal radiation energy due to SWCNTs on MHD nanofluid flow in the presence of seawater/water: Lie group transformation, Ain Shams Eng J (2016), http://dx.doi.org/10.1016/j.asej.2016.04.022

field and thermal energy radiation. The water and seawater based SWCNTs have been considered in the present work. Governing PDEs are converted into coupled nonlinear ODEs and then solved numerically by shooting technique with Runge–Kutta–Fehlberg method.

## 2. Mathematical analysis

Consider a two dimensional, MHD unsteady boundary layer Darcy flow of an incompressible viscous nanofluid over a porous wedge sheet with variable stream conditions (see Fig. 1). The temperature at the wedge sheet and ambient takes the constant value $T_w$ and $T_\infty$ respectively and the magnetic strength $B_0$ is applied parallel to the $y$-axis. The nanofluid is a water/seawater based nanoparticles Cu, $Al_2O_3$ and SWCNTs. It is assumed that the base fluids (water/seawater) and the suspended nanoparticles are in thermal equilibrium. The thermophysical properties of the nanofluids are presented in Table 1 [41,40,47]. The porous wedge is assumed to be transparent and in thermal equilibrium with the nanofluids. Non reflecting absorbing ideally transparent wedge sheet observes an incident radiation flux of intensity $q''_{rad}$. The thermal radiation flux penetrates the plate and is absorbed in an adjacent fluid of absorption coefficient. The induced magnetic field produced by the fluid motion is justified as $\vec{B} = (0, B_0, 0)$ and the effect of polarization of fluid is negligible, $\vec{E} = (0, 0, 0)$. Based on the assumption, the momentum and energy equations can be expressed as [42]

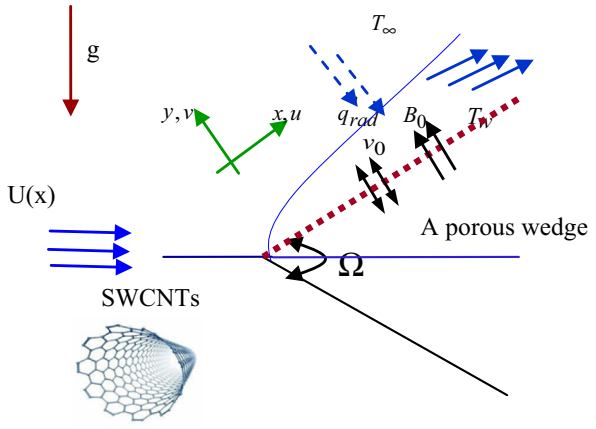


**Figure 1** System of flow model over a porous wedge sheet.

$$\frac{\partial \bar{u}}{\partial \bar{x}} + \frac{\partial \bar{v}}{\partial \bar{y}} = 0 \tag{1}$$

$$\frac{\partial \bar{u}}{\partial \bar{t}} + \bar{u}\frac{\partial \bar{u}}{\partial \bar{x}} + \bar{v}\frac{\partial \bar{u}}{\partial \bar{y}} = \frac{1}{\rho_{nf}}\left[\left(\frac{\partial U}{\partial t} + U\frac{\partial U}{\partial x}\right)\rho_{nf} + \mu_{f_n}\frac{\partial^2 \bar{u}}{\partial \bar{y}^2} + (\rho\beta)_{nf}\bar{g}(T - T_\infty)\sin\frac{\Omega}{2} - \left(\sigma B_0^2 + \frac{\nu_{nf}}{K}\rho_{nf}\right)(\bar{u} - U)\right] \tag{2}$$

$$\frac{\partial T}{\partial \bar{t}} + \bar{u}\frac{\partial T}{\partial \bar{x}} + \bar{v}\frac{\partial T}{\partial \bar{y}} = \frac{1}{(\rho c_p)_{nf}}\left(k_{nf}\frac{\partial^2 T}{\partial \bar{y}^2} - \frac{\partial q''_{rad}}{\partial y} - Q_0(T - T_\infty)\right) \tag{3}$$

Darcy's law is a constitutive equation that describes the flow of a nanofluid through a porous wedge cone. The term $Q_0(T_\infty - T)$ is assumed to be the amount of heat source/sink per unit volume, $Q_0$ is a constant and it is assumed to be the amount of heat generated ($Q_0 > 0$)/absorbed ($Q_0 < 0$) per unit volume. Using Rosseland approximation for thermal radiation, $q''_{rad} = -\frac{4\sigma_1}{3k^*}\frac{\partial T^4}{\partial y}$, $\sigma_1$ – Stefan–Boltzmann constant, $k^*$ – mean absorption coefficient. $u$ and $v$ – velocity components along the $x$-*axis* and $y$-*axis*, respectively, $T$ – temperature of the base fluid, $\beta_{nf}$ – thermal expansion coefficient of the nanofluid, $\rho_{nf}$ – density of nanofluid, $\nu_{nf}$ – kinematic viscosity of nanofluid and $\alpha_{nf}$ – thermal diffusivity of nanofluid which are defined as [41],

$$\nu_{nf} = \frac{\mu_{nf}}{\rho_{nf}}, \quad (\rho\beta)_{nf} = (1-\varphi)(\rho\beta)_f + \varphi(\rho\beta)_s, \quad \alpha_{nf} = \frac{k_{nf}}{(\rho c_p)_{nf}},$$

$$(\rho c_p)_{nf} = (1-\varphi)(\rho c_p)_f + \varphi(\rho c_p)_s,$$
$$\frac{k_{nf}}{k_f} = \left\{\frac{(k_s + 2k_f) - 2\varphi(k_f - k_s)}{(k_s + 2k_f) + 2\varphi(k_f - k_s)}\right\} \tag{4}$$

$\nu_f$ – kinematic viscosity of base fluid, $\varphi$ – nanoparticle volume fraction, $(\rho c_p)_{nf}$ – effective heat capacity of a nanoparticle, $k_{nf}$ – thermal conductivity of nanofluid, $k_f$ and $k_s$ – thermal conductivities of the base fluid and nanoparticles while $\rho_f$ and $\rho_s$ – densities of the base fluid and nanoparticles. The corresponding boundary conditions are stated as

$$\bar{u} = 0, \quad \bar{v} = -v_0, \quad T = T_w + c_1 x^{n_1} \text{ at } \bar{y} = 0;$$

$$\bar{u} \to U = \frac{\nu_f x^m}{\delta^{m+1}}, \quad T \to T_\infty \text{ as } \bar{y} \to \infty \tag{5}$$

$c_1$ and $n_1$ (power index) are constants and $v_0$ is the suction ($v_0 > 0$) or injection ($v_0 < 0$) velocity of the fluid at the wedge. The potential flow velocity can be written as $U(x,t) = \frac{\nu_f x^m}{\delta^{m+1}}$, $\beta_1 = \frac{2m}{1+m}$ (see in Sattar [43]), $\delta$ – time-dependent length scale which is considered to be $\delta = \delta(t)$ and $\beta_1$ – Hartree pressure

**Table 1** Thermophysical properties of fluid and nanoparticles.

| | $\rho$ (kg/m$^3$) | $c_p$ (J/kg K) | $k$ (W/m K) | $\beta \times 10^{-5}$ (K$^{-1}$) | $\alpha \times 10^{-7}$ (m$^2$/s) |
|---|---|---|---|---|---|
| Pure water | 997.1 | 4179 | 0.613 | 21 | 1.47 |
| Seawater | 1021 | 4000 | 0.6015 | 4.181 | 1.46 |
| Copper (Cu) | 8933 | 385 | 401 | 1.67 | 1163.1 |
| Alumina ($Al_2O_3$) | 3970 | 765 | 40 | 0.85 | 131.7 |
| Titanium ($TiO_2$) | 4250 | 6862 | 8.9538 | 0.9 | 30.7 |
| SWCNTs | 2600 | 425 | 6600 | 0.33 | 2.0 |

gradient parameter that tends to $\beta_1 = \frac{\Omega}{\pi}$ for a total angle $\Omega$ of the wedge. By Kafoussias and Nanousis [44], the stream functions are defined as

$$\eta = y\sqrt{\frac{(1+m)}{2}}\sqrt{\frac{x^{m-1}}{\delta^{m+1}}}, \quad \psi = \sqrt{\frac{2}{1+m}}\frac{v_f x^{\frac{m+1}{2}}}{\delta^{\frac{m+1}{2}}} f(\eta),$$

$$\theta = \frac{T - T_\infty}{T_w - T_\infty}, \quad u = \frac{\partial \psi}{\partial y} \text{ and } v = -\frac{\partial \psi}{\partial x} \tag{6}$$

Eqs. (2) and (3) become

$$\frac{\partial^2\psi}{\partial t \partial y} + \frac{\partial \psi}{\partial y}\frac{\partial^2 \psi}{\partial x \partial y} - \frac{\partial \psi}{\partial x}\frac{\partial^2 \psi}{\partial y^2} = \frac{1}{\left(1-\zeta+\zeta\frac{\rho_s}{\rho_f}\right)}\left[\left\{\left(1-\zeta+\zeta\frac{(\rho\beta)_s}{(\rho\beta)_f}\right)g(\rho\beta)_f \Delta T \sin\frac{\Omega}{2}\theta\right\} + \frac{v_f}{(1-\zeta)^{2.5}}\frac{\partial^3\psi}{\partial y^3} + U\frac{dU}{dx} - \left((1-\zeta)^{2.5}\frac{\sigma B_0^2}{\rho_{nf}} + \frac{v_{nf}}{K}\right)(u-U)\right] \tag{7}$$

$$\frac{\partial T}{\partial t} + \frac{\partial \psi}{\partial y}\frac{\partial T}{\partial x} - \frac{\partial \psi}{\partial x}\frac{\partial T}{\partial y} = \frac{1}{1-\zeta+\zeta\frac{(\rho c_p)_s}{(\rho c_p)_f}}\left[\frac{1}{Pr}\left\{\frac{k_{f_n}}{k_f}\frac{\partial^2 T}{\partial y^2} + \frac{4}{3}N((C_T+T)^3\theta')'\right\} - \frac{Q_0 \Delta T}{(\rho c_p)_f}\theta\right] \tag{8}$$

Boundary conditions

$$\frac{\partial \psi}{\partial y} = 0, \quad \frac{\partial \psi}{\partial x} = -V_0, \quad T = T_w \text{ at } y = 0;$$
$$\frac{\partial \psi}{\partial y} \to \frac{v x^m}{\delta^{m+1}}, \quad T \to T_\infty \text{ as } \bar{y} \to \infty \tag{9}$$

$C_T = \frac{T_\infty}{T_w} - T_\infty$ – temperature ratio where $C_T$ assumes very small constant by its definition as $T_w - T_\infty \gg T_\infty$. In this study, it is assigned the value $C_T = 0.1$, Murthy et al. [45].

The symmetry groups of Eqs. (7) and (8) are calculated using classical Lie group analysis and it is defined as

$$x^* = x + \varepsilon\xi_1(x,y,\psi,\theta), \quad y^* = y + \varepsilon\xi_2(x,y,\psi,\theta),$$
$$\psi^* = \psi + \varepsilon\mu_1(x,y,\psi,\theta), \quad \theta^* = \theta + \varepsilon\mu_2(x,y,\psi,\theta) \tag{10}$$

By algebraic approaches, the formation of infinitesimals is

$$\xi_1 = c_1 x + c_2, \quad \xi_2 = g(x), \quad \mu_1 = c_3\psi + c_4 \text{ and } \mu_2 = c_5\theta \tag{11}$$

$g(x)$-arbitrary function and the infinitesimal generators are defined as

$$X_1 = x\frac{\partial}{\partial x} + g(x)\frac{\partial}{\partial y} + \psi\frac{\partial}{\partial \psi} + \theta\frac{\partial}{\partial \theta},$$
$$X_2 = \frac{\partial}{\partial x} + g(x)\frac{\partial}{\partial y}, \quad X_3 = g(x)\frac{\partial}{\partial y} + \frac{\partial}{\partial \psi} \tag{12}$$

The given PDEs are transformed by a special case of Lie symmetry group transformations viz. one-parameter infinitesimal Lie group of transformation into a system of ODEs.

The characteristic equations are

$$\frac{dx}{x} = \frac{dy}{0} = \frac{d\psi}{\psi} = \frac{d\theta}{\theta} \tag{13}$$

Solving the equations, we get

$$\eta = y, \quad \psi = xf(\eta) \text{ and } \theta = x\theta(\eta) \text{ where } \eta = \eta(x,t) \tag{14}$$

Eqs. (7) and (8) become

$$f''' + \left(1-\zeta+\zeta\frac{\rho_s}{\rho_f}\right)(1-\zeta)^{2.5}\xi^2[\lambda_v(-2+2f'+\eta f'') + ff'' + \frac{2m}{m+1}(1-f'^2)] + \frac{2}{m+1}\left[\left\{\left(1-\zeta+\zeta\frac{(\rho\beta)_s}{(\rho\beta)_f}\right)\right\} \times \xi^{\frac{1}{1-m}}(1-\zeta)^{2.5}\gamma\sin\frac{\Omega}{2}\theta - (M(1-\zeta)^{2.5}+\lambda)(f'-1)\right] + \left(1-\zeta+\zeta\frac{\rho_s}{\rho_f}\right)(1-\zeta)^{2.5}\frac{1-m}{1=m}\xi\frac{\partial f}{\partial \xi}\left(\frac{\partial f}{\partial \eta} - \frac{\partial^2 f}{\partial \eta^2}\right) = 0 \tag{15}$$

$$\theta'' + \frac{4}{3}\frac{k_f}{k_{f_n}}N\{(C_T+\theta)^3\theta'\}' - Pr\left\{1-\zeta+\zeta\frac{(\rho c_p)_s}{(\rho c_p)_f}\right\}\frac{k_f}{k_{f_n}}\left[\frac{2n_1}{m+1}f\theta - f\theta' + \lambda_v\eta\theta' + \frac{2}{1+m}\delta_1\theta + \frac{1-m}{1+m}\left\{\xi\frac{\partial\theta}{\partial\xi}\frac{\partial f}{\partial\eta} - \xi\frac{\partial f}{\partial\xi}\frac{\partial\theta}{\partial\eta}\right\}\right] = 0 \tag{16}$$

Boundary conditions take the form

$$\frac{\partial f}{\partial \eta} = 0, \quad \frac{m+1}{2}f + \frac{1-m}{2}\xi\frac{\partial f}{\partial \xi} = -S, \quad \theta = 1 \text{ at } \eta = 0$$
$$\text{and } \frac{\partial f}{\partial \eta} = 1, \quad \theta \to 0 \text{ as } \eta \to \infty \tag{17}$$

$Pr = \frac{v_f}{\alpha_f}$ is the Prandtl number, $\lambda = \frac{\delta^{m+1}}{Kk^2}$ is the porous media parameter, $N = \frac{4\sigma_1\theta_w^3}{k_{nf}k^*}$ – thermal radiation parameter, $\theta_w = \frac{1}{T_w - T_\infty}$. $\gamma = \frac{g(\rho\beta)_f \Delta T}{\rho_f U^2 k^{\frac{2}{1-m}}}$ is the buoyancy or natural convection parameter, $\delta_1 = \frac{Q_0 v_f^2}{k_f U^2}\Delta T$ is the heat source/sink parameter and $M = \frac{\sigma B_0^2}{\mu_f}\frac{\delta^{m+1}}{k^2}$ is the magnetic parameter. $S = -V_0\sqrt{\frac{(1+m)x}{2vU}}$ is the suction parameter if $S > 0$ and injection if $S < 0$ and $\xi = k\, x^{\frac{1-m}{2}}$, Kafoussias and Nanousis [44], is the dimensionless distance along the wedge ($\xi > 0$). In this system of equations, it is obvious that the nonsimilarity aspects of the problem are embodied in the terms containing partial derivatives with respect to $\xi$. This problem does not admit similarity solutions. Thus, with $\xi$-derivative terms retained in the system of equations, it is necessary to employ a numerical scheme suitable for partial differential equations for the solution. Formulation of the system of equations for the local nonsimilarity model with reference to the present problem will now be discussed. At the first level of truncation, the terms accompanied by $\xi\frac{\partial}{\partial\xi}$ are small. This is particularly true when ($\xi \ll 1$). Thus the terms with $\xi\frac{\partial}{\partial\xi}$ on the right-hand sides of Eqs. (15) and (16) are deleted to get the following system of equations:

$$f''' + \left(1-\zeta+\zeta\frac{\rho_s}{\rho_f}\right)(1-\zeta)^{2.5}[\lambda_v(-2+2f'+\eta f'') + ff'' + \frac{2m}{m+1}(1-f'^2)] + \frac{2}{m+1}\left[\left\{\left(1-\zeta+\zeta\frac{(\rho\beta)_s}{(\rho\beta)_f}\right)\right\} \times (1-\zeta)^{2.5}\gamma\sin\frac{\Omega}{2}\theta - (M(1-\zeta)^{2.5}+\lambda)(f'-1)\right] = 0 \tag{18}$$

$$\theta'' + \frac{4}{3}\frac{k_f}{k_{f_n}}N\left\{(C_T+\theta)^3\theta'\right\}' - Pr\left\{1-\zeta+\zeta\frac{(\rho c_p)_s}{(\rho c_p)_f}\right\}\frac{k_f}{k_{f_n}}\left[\frac{2n_1}{m+1}f'\theta - f\theta' + \lambda_v\eta\theta' + \frac{2}{1+m}\delta_1\theta\right] = 0 \tag{19}$$

Boundary conditions

$$f' = 0, \quad f = -\frac{2S}{m+1}, \quad \theta = 1 \text{ at } \eta = 0 \text{ and } f' = 1,$$
$$\theta \to 0 \text{ as } \eta \to \infty \tag{20}$$

Let $\lambda_v = \frac{c}{x^{m-1}}$, where $c = \frac{\delta^m}{\nu_f}\frac{\partial \delta}{\partial t}$ and integrating, $\delta = [c(m+1)\nu_f t]^{\frac{1}{m+1}}$. When $c = 2$ and $m = 1$ in $\delta$, we get $\delta = 2\sqrt{\nu_f t}$ which obtains that the parameter $\delta$ can be compared with the well established scaling parameter for the unsteady boundary layer problems (see Schlichting [46]). The skin friction coefficient and the Nusselt number are defined as

$$C_f = \frac{\mu_{f_n}}{\rho_f U^2}\left(\frac{\partial u}{\partial y}\right)_{\text{at } y=0} = -\frac{1}{(1-\zeta)^{2.5}}(Rex)^{-\frac{1}{2}} f''(0) \tag{21}$$

$$Nu_x = \frac{xk_{f_n}}{k_f(T_w - T_\infty)}\left(\frac{\partial T}{\partial y}\right)_{\text{at } y=0} = -(Rex)^{\frac{1}{2}}\frac{k_{f_n}}{k_f}\theta'(0)\left[1 + \frac{4}{3}N(C_T + \theta(0))^3\right] \tag{22}$$

$Re = \frac{Ux}{\nu_f}$ – local Reynolds number.

## 3. Numerical solution

By using DSolve subroutine command in MAPLE 18 we can get the solution for Eqs. (18)–(20) with trial and error basis. This software consists of fourth–fifth order Runge–Kutta–Fehlberg method with shooting technique. The numerical results the dimensionless velocity, temperature, skin friction and the rate of heat transfer in the presence of SWCNT–water and SWCNT–seawater are obtained.

## 4. Results and discussion

Eqs. (18) and (19) with boundary conditions (20) have been solved numerically for some values of the governing parameters $Pr$, $\zeta$, $m$, $\lambda$, $\delta 1$, $n_1$, $\lambda_v$ and $N$ using Maple 18. $\gamma \gg 1.0$, $\gamma = 1.0$ and $\gamma \ll 1.0$ represent to free convection, mixed convection and forced convection. In this work we have assumed $\gamma = 100$. Validating our technique, $f''(0)$ is compared with those of Rizwan et al. [41] and found that they are in good agreement, see Table 2. Thermophysical properties of the fluid and the nanoparticles are defined in Table 1 [41,40,47].

It is predicted from Fig. 2 that the agreement with the solution of temperature profile for various values of nanoparticle volume fraction significantly correlates with Fig. 8(a) of Rizwan et al. [41].

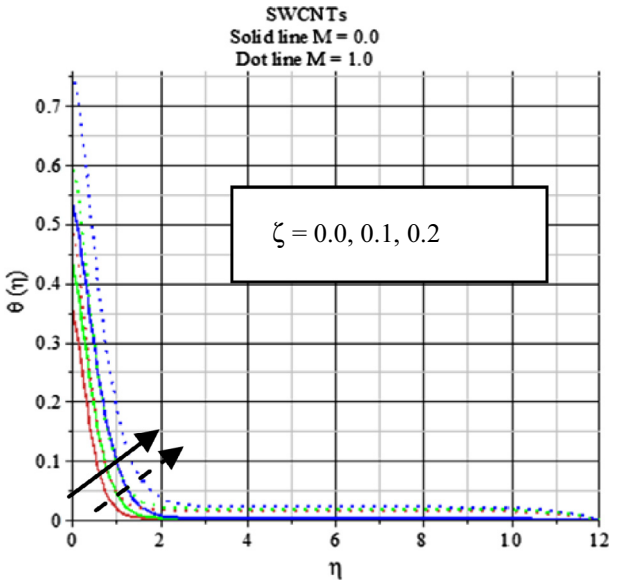


**Figure 2** Comparison of temperature profile for $\zeta$ with Fig. 8(a) of Rizwan et al. [41].

Fig. 3 presents the velocity and temperature profiles for different values of the thermal radiation parameter $N$ in the presence of SWCNTs–seawater and SWCNTs–water. It is noticed that the velocity and the temperature of water and seawater based SWCNTs increase significantly whereas the rate of heat transfer decreases with increase of the radiation parameter $N$ ($0.5 \leqslant N \leqslant 1.5$). This is due to the combined effects of thermal conductivity and density of the SWCNTs–nanofluid. It is interesting to note that rate of heat transfer for SWCNTs–seawater is higher than that of SWCNTs–water (Table 3) and the thermal boundary layer thickness for SWCNTs–seawater is lower as compared to SWCNTs–water. Fig. 4 presents the velocity and the temperature profiles for different values of magnetic parameter in the presence of water and seawater based SWCNTs. It is clearly shown that the velocity of the nanofluids (SWCNTs–seawater and SWCNTs–water) decreases and the thermal boundary layer thickness for SWCNTs–seawater is lower than that of SWCNTs–water with increase of magnetic strength $M$ ($1.0 \leqslant M \leqslant 10.0$) because of the combined effects of thermal and electric conductivities of the nanofluid. The effects of a transverse magnetic field to an electrically conducting fluid give rise to a resistive-type force called the Lorentz force. This force clearly indicates that the

**Table 2** Comparison of skin friction coefficient $-C_f Re_x^{\frac{1}{2}}$ for various values of $M$.

| | $\zeta$ | Rizwan et al. [41] $\beta = 0.5$ | | Present work $\beta = 0.5$ | |
|---|---|---|---|---|---|
| | | $M = 0$ | $M = 0.5$ | $M = 0$ | $M = 0.5$ |
| SWCNTs–water | 0.0 | 0.5912 | 0.6495 | 0.591178452 | 0.649493428 |
| | 0.1 | 0.6680 | 0.7242 | 0.667965268 | 0.724248769 |
| | 0.2 | 0.7504 | 0.8051 | 0.750374192 | 0.805072871 |
| MWCNTs–water | 0.0 | 0.5912 | 0.6495 | 0.591194527 | 0.649522965 |
| | 0.1 | 0.6508 | 0.7106 | 0.650793523 | 0.710573241 |
| | 0.2 | 0.7180 | 0.7795 | 0.717956234 | 0.779531892 |

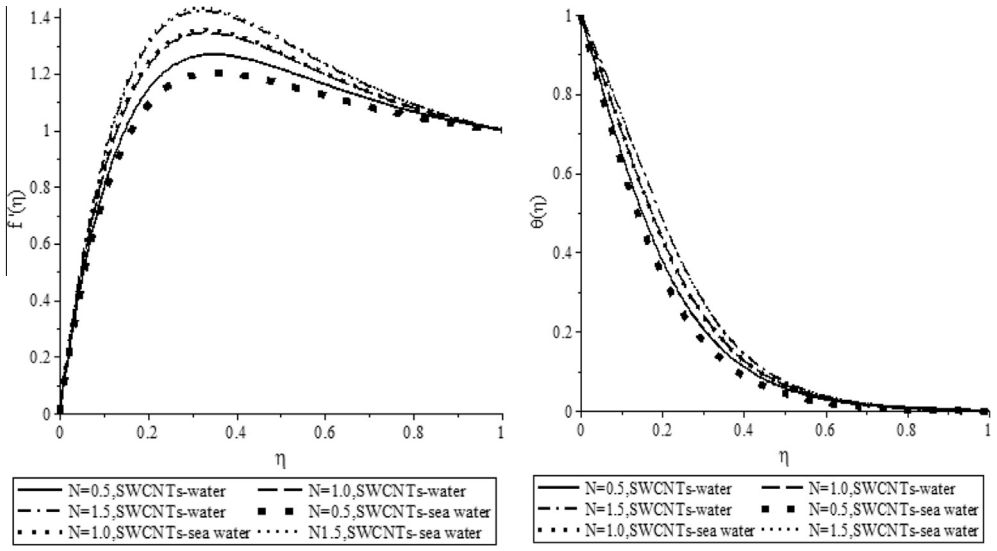


**Figure 3** Thermal radiation effects on velocity and temperature profiles.

**Table 3** $f''(0)$ and $-\theta'(0)$ for different values of $N$ with $Pr = 6.2,\ \lambda = 0.5,\ \delta = 0.5,\ \delta 1 = 1.0,\ M = 5.0$.

| | $N$ | $f''(0)$ | $-\theta'(0)$ |
|---|---|---|---|
| SWCNTs–water | 0.1 | 10.78515452805541 | 4.44071358942363 |
| | 1.0 | 12.01004734012169 | 2.56980496118636 |
| | 1.5 | 12.54880714059170 | 2.15043460939386 |
| SWCNTs–seawater | 0.1 | 10.47780500700737 | 4.87246624249648 |
| | 1.0 | 12.14490973744439 | 2.57556285092944 |
| | 1.5 | 12.69131496777138 | 2.15560604210558 |

**Table 4** $f''(0)$ and $-\theta'(0)$ for different values of $M$ with $Pr = 6.2,\ \lambda = 0.5,\ \delta = 0.5,\ \delta 1 = 1.0,\ N = 1.0$.

| | $M$ | $f''(0)$ | $-\theta'(0)$ |
|---|---|---|---|
| SWCNTs–water | 1.0 | 11.46837881046136 | 3.327802520956691 |
| | 5.0 | 11.41054185295425 | 3.301552163607098 |
| | 10.0 | 11.51920648179646 | 3.285734958955961 |
| SWCNTs–seawater | 1.0 | 11.05998859748521 | 3.626179963621877 |
| | 5.0 | 11.53659929438686 | 3.308355416963920 |
| | 10.0 | 11.63507422022600 | 3.291863107156541 |

transverse magnetic field opposes the transport phenomena and it has the tendency to slow down the motion of the fluid and to accelerate its temperature profiles. In addition, the virtue of viscosity also contributes to the flow resistance of the nanofluid. It is also observed that the rate of heat transfer for SWCNTs–seawater is higher than that of SWCNTs–water, Table 4. Effects of heat source ($\delta 1 > 0$) on velocity and temperature distribution in the presence of water and seawater based SWCNTs are shown in Fig. 5. The presence of heat source in the boundary layer generates energy which causes

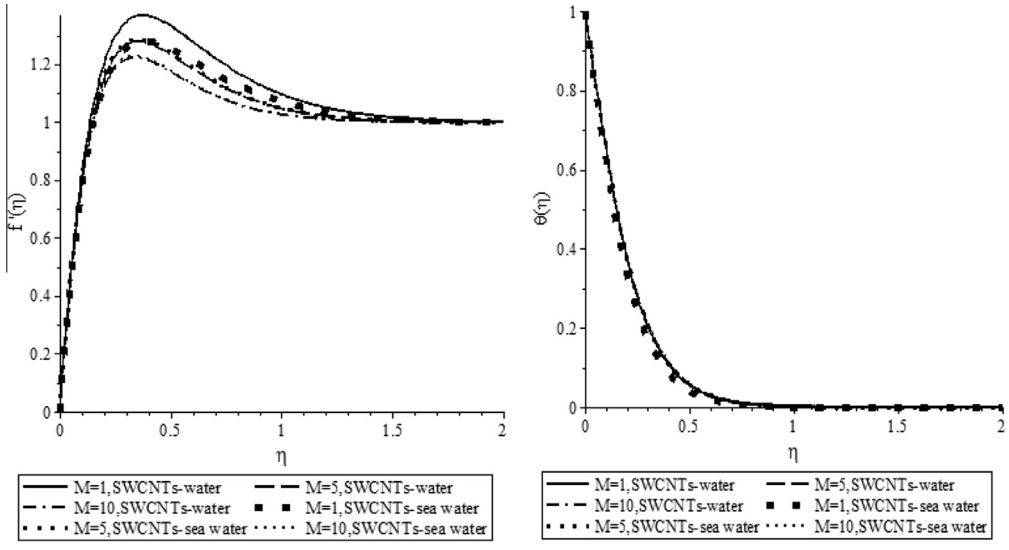


**Figure 4** Magnetic effects on velocity and temperature profiles.

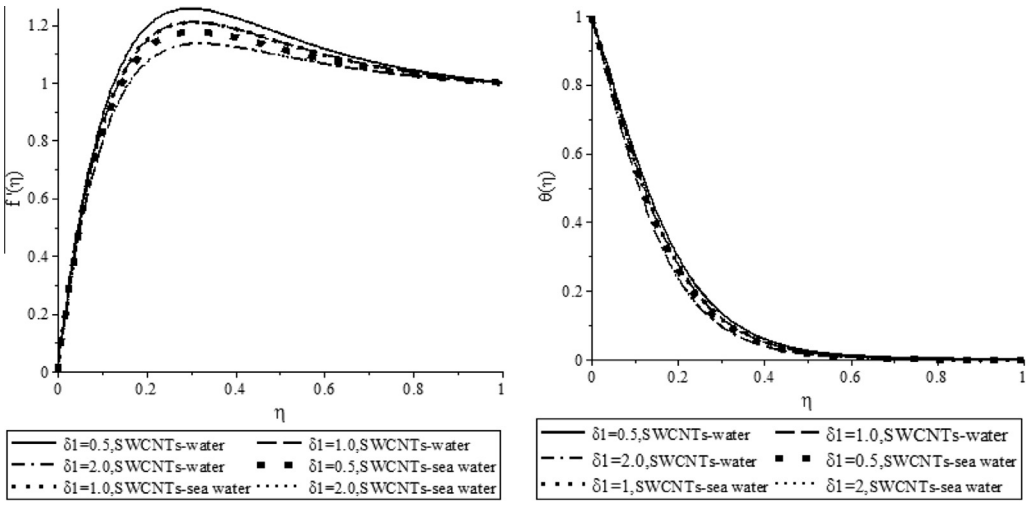


**Figure 5** Heat source effects on velocity and temperature profiles.

**Table 5** $f''(0)$ and $-\theta'(0)$ for different values of $\delta 1$ with $Pr = 6.2,\ \lambda = 0.5,\ \delta = 0.5,\ M = 1.0,\ N = 1.0$.

| | $\delta 1$ | $f''(0)$ | $-\theta'(0)$ |
|---|---|---|---|
| SWCNTs–water | 0.5 | 11.37755577688759 | 3.319610279719555 |
| | 1.0 | 15.22112322110225 | 1.311348595211690 |
| | 2.0 | 10.40295062182951 | 4.047739154648341 |
| SWCNTs–seawater | 0.5 | 10.99108927319695 | 3.619438710017548 |
| | 1.0 | 11.15065548558862 | 3.583203927185552 |
| | 2.0 | 10.53025973448391 | 4.053370538109227 |

**Table 6** $f''(0)$ and $-\theta'(0)$ for different values of $\lambda$ with $Pr = 6.2, \delta 1 = 1.0, \delta = 0.5, M = 1.0, N = 1.0$.

| | $\lambda$ | $f''(0)$ | $-\theta'(0)$ |
|---|---|---|---|
| SWCNTs–water | 0.5 | 11.04231526747509 | 3.566038443801494 |
| | 1.0 | 11.69371791531883 | 2.775492013091292 |
| | 2.0 | 11.10555621327483 | 3.560176781255234 |
| SWCNTs–seawater | 0.5 | 10.71296891958325 | 3.893664523230942 |
| | 1.0 | 11.19124567801182 | 3.569031305982667 |
| | 2.0 | 11.22517248803293 | 3.566059988320378 |

the velocity and temperature of the nanofluids (water and seawater based SWCNTs) to increase firstly and then decrease whereas the rate of heat transfer firstly decreases and then increases but the skin friction firstly increases and then decreases with increase of heat source, Table 5. It is interesting to note that the rate of heat transfer for SWCNTs–seawater is stronger than that of SWCNTs–water.

Fig. 6 illustrates the typical velocity and temperature profiles as obtained by varying the porosity parameter for the case of SWCNTs–seawater and SWCNTs–water, respectively. It is clearly shown that the velocity and the temperature of the nanofluids gradually increase and then decrease with increase of porosity parameter but the rate of heat transfer for SWCNTs–water firstly decreases and then increases whereas

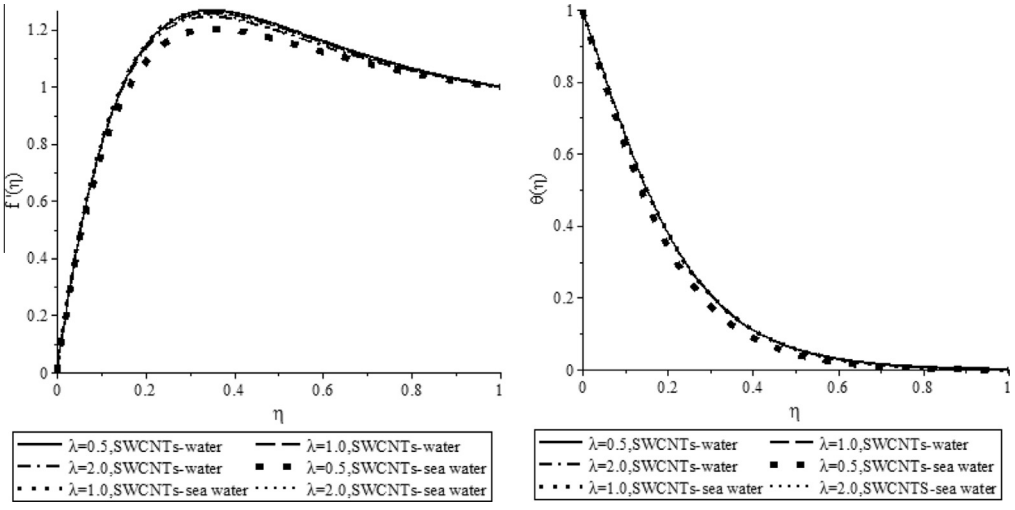


**Figure 6** Porosity effects on velocity and temperature profiles.

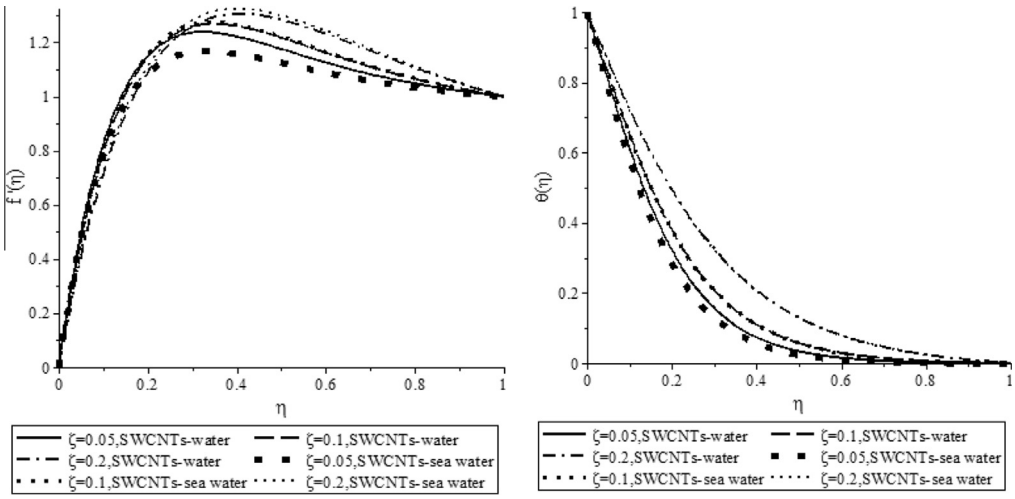


**Figure 7** Nanoparticle volume fraction on velocity and temperature profiles.

**Table 7** $f''(0)$ and $-\theta'(0)$ for different values of $\zeta$ with $Pr = 6.2, \delta 1 = 1.0, \delta = 0.5, M = 1.0, N = 1.0$.

| | $\zeta$ | $f''(0)$ | $-\theta'(0)$ |
|---|---|---|---|
| SWCNTs–water | 0.05 | 11.9060402546369 | 3.92156368275020 |
| | 0.10 | 11.0531623230024 | 3.56460450073797 |
| | 0.20 | 9.30511366740325 | 2.86217226965315 |
| SWCNTs–seawater | 0.05 | 11.4573541325429 | 4.29156742368451 |
| | 0.10 | 11.1772416291270 | 3.57075633104794 |
| | 0.20 | 9.53683830358729 | 2.87375282410418 |

**Table 8** $f''(0)$ and $-\theta'(0)$ for different nanoparticles in water and seawater with $Pr = 6.2, \delta 1 = 1.0, \delta = 0.5, M = 1.0, N = 1.0$.

| | Nanoparticles | $f''(0)$ | $-\theta'(0)$ |
|---|---|---|---|
| Water | Cu | 11.7950993251236 | 3.72514561420155 |
| | $Al_2O_3$ | 11.0390776462575 | 3.69626924128355 |
| | SWCNTs | 11.0531623230023 | 3.56460450073796 |
| Seawater | Cu | 13.3634097847336 | 4.14766549361491 |
| | $Al_2O_3$ | 11.5691100313522 | 3.70074897606376 |
| | SWCNTs | 11.1772416291270 | 3.57075633104792 |

it decreases for SWCNTs–seawater with increase of porosity parameter, Table 6. The effect of nanoparticle volume fraction of added singe walled carbon nanotubes (SWCNTS) on flow and temperature fields of the water and seawater is presented in Fig. 7. It is clear that the velocity of nanofluids (SWCNTs–water and SWCNTs–seawater) firstly decreases and then increases while the temperature of the nanofluids increases with increase of nanoparticle volume fraction. It is also predicted that the rate of heat transfer decreases (Table 7) with increase of nanoparticle volume fraction and also the rate of heat transfer for seawater based SWCNTs is stronger than that of SWCNTs–water.

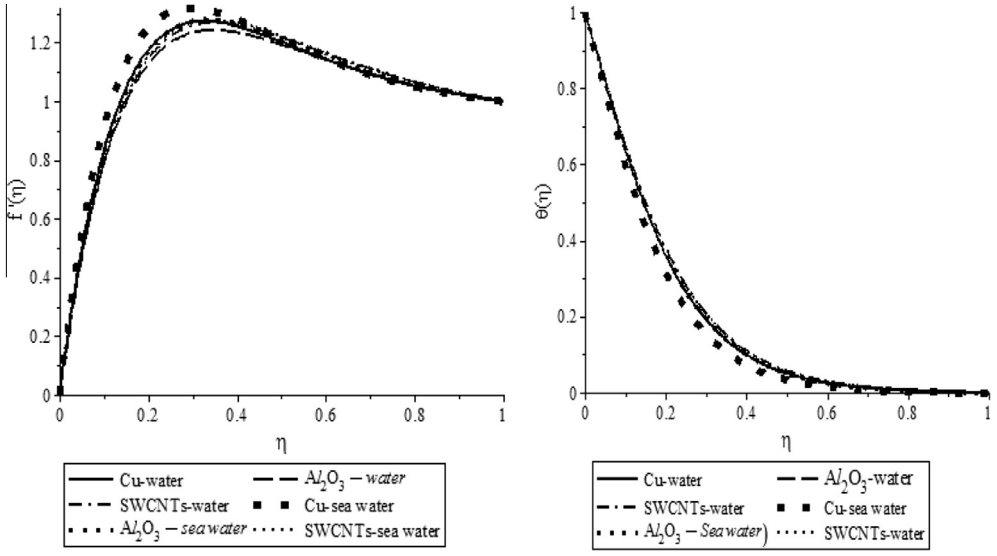


**Figure 8** Different nanoparticles – water effects on velocity and temperature profiles.

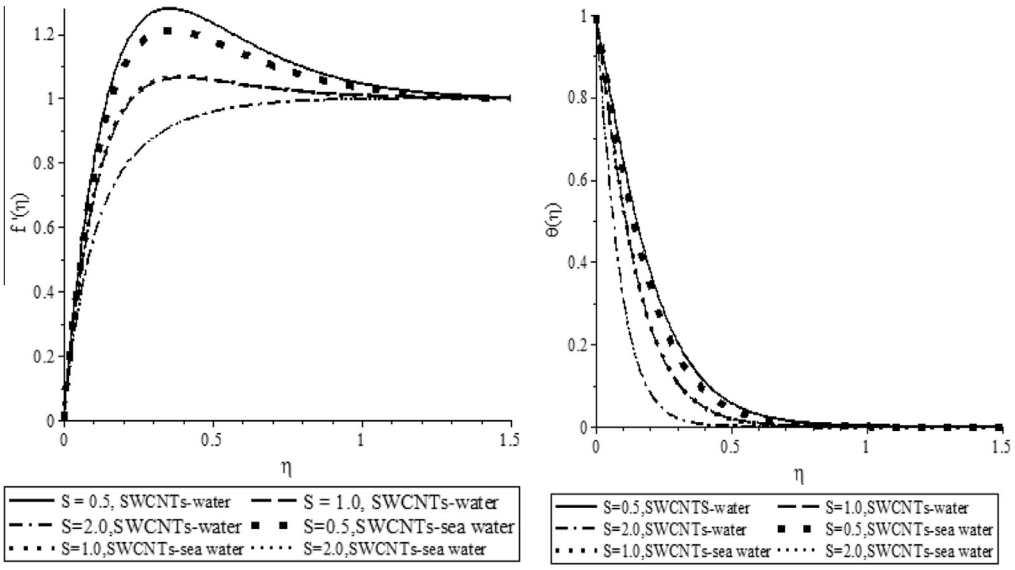


**Figure 9** Suction effects on velocity and temperature profiles.

**Table 9** $f''(0)$ and $-\theta'(0)$ for different values of $S > 0$ with $Pr = 6.2$, $\delta 1 = 1.0$, $\delta = 0.5$, $M = 1.0$, $N = 1.0$.

| | $S$ | $f''(0)$ | $-\theta'(0)$ |
|---|---|---|---|
| SWCNTs–water | 0.5 | 11.0827668898851 | 3.56647923488613 |
| | 1.0 | 10.1126864378420 | 4.97996433455483 |
| | 2.0 | 9.00925245181533 | 8.47993106975987 |
| SWCNTs–seawater | 0.5 | 10.7530200385213 | 3.89437180975383 |
| | 1.0 | 10.2145846282221 | 4.98527966177432 |
| | 2.0 | 9.07130618912964 | 8.48521131866359 |

The effect of different nanoparticles in the presence of water and seawater on the dimensionless velocity and temperature profiles has been displayed in Fig. 8. It is observed that the velocity of the nanofluid firstly decreases and then increases and the temperature of the nanofluids increases whereas the rate of heat transfer decreases (Table 8) with the increase of the said sequences of water and seawater based Cu, $Al_2O_3$ and SWCNTs. It is noticed that the momentum and thermal boundary layer thickness of SWCNTs–seawater is stronger than that of SWCNTs–water. It is also observed that the skin friction and the rate of heat transfer of Cu–seawater are stronger than those of all the other mixtures in the flow regime. Fig. 9 depicts the influence of the suction parameter $S$ on the velocity and temperature profiles in the boundary layer when the magnetic field is uniform. It is seen that the velocity and the temperature of the nanofluids (SWCNTs–seawater and SWCNTs–water) decrease and the rate of heat transfer increases (Table 9) with increase of suction parameter. It is also observed that the momentum and thermal boundary layer thickness for SWCNTs–water is stronger than that of SWCNTs–water. However, the exact opposite behavior is produced by imposition of wall fluid blowing or injection.

## 5. Conclusion

The purpose of the study is worthwhile to submit the comparison among the SWCNTs in the presence of water and seawater for absolute skin friction and the rate of heat transfer. In addition, the effect of various values of existing parameters on velocity and temperature is discussed graphically and quantitatively. The main observation of present study is as follows:

- Momentum and thermal boundary layer thickness for SWCNTs–seawater is stronger than that of SWCNTs–water with increase of the radiation parameter because of low thermal conductivity of seawater.
- Thermal boundary layer thickness for SWCNTs–seawater is lower as compared to SWCNTs–water with increase of magnetic parameter. It is clearly demonstrated that the effect of thermal conductivity of SWCNTs–seawater with magnetic field can be treated as a means of controlling the flow and heat transfer of the nanofluids.
- It is interesting to note that the rate of heat transfer for SWCNTs–seawater is stronger than that of SWCNTs–water with increase of heat source because of the low strength of heat capacitance of seawater.
- It is clearly shown that the rate of heat transfer SWCNTs–seawater is better than that of SWCNTs–water with increase of porosity parameter because of the combined effects of kinematic viscosity of SWCNTs–seawater with permeability of wedge sheet.
- The strength of rate of heat transfer of SWCNTs–seawater is higher than that of SWCNTs–water with increase of nanoparticle volume fraction and suction parameters since the heated fluid is pushed toward the wall where the buoyancy forces can act to retard the fluid due to high influence of the viscosity of seawater.
- It is concluded that the rate of heat transfer of Cu–seawater is significantly stronger than all the other mixtures in the flow regime because of the combined effects of density of copper and seawater.

Seawater based SWCNTs have attracted good attention on thermal boundary layer flow regime because of their remarkable properties. Indeed, it was proved that the seawater based single walled carbon nanotubes have a high thermal and

Please cite this article in press as: Kandasamy R et al., Thermal radiation energy due to SWCNTs on MHD nanofluid flow in the presence of seawater/water: Lie group transformation, Ain Shams Eng J (2016), http://dx.doi.org/10.1016/j.asej.2016.04.022

electrical conductivity and efficient mechanical properties. SWCNTs–seawater is expected to exhibit better heat transfer properties compared with conventional heat transfer of SWCNTs–water.

## References

[1] Ebbesen TW, editor. Carbon nanotubes preparation and properties. New York: CRC Press; 1997.
[2] Cai D, Mataraza JM, Qin ZH, Huang Z, Huang J, Chiles TC, Carnahan D, Kempa K, Ren Z. Highly efficient molecular delivery into mammalian cells using carbon nanotube spearing. Nat Methods 2005;2:449–54.
[3] Pastorin G, Wu W, Wieckowski S, Briand JP, Kostarelos K, Prato M, Bianco A. Double functionalization of carbon nanotubes for multimodal drug delivery. Chem Commun 2006;11:1182–4;
Wang XY, Wang X, Sheng GG. The coupling vibration of fluid-filled carbon nanotubes. J Phys D 2007;40:2563.
[4] Coleman JN, Curran S, Dalton AB. Nanostructured materials for advanced technological applications. Phys Rev B 1998;58:7492–7.
[5] Ando Y, Zhao X, Shimoyama H, Sakai G, Kaneto K. Physical properties of multiwalled carbon nanotubes. Int J Inorg Mater 1999;1:77–81.
[6] Xie SS, Li WZ, Pan ZW, Chang BH, Sun LF. Mechanical and physical properties on carbon nanotube. J Phys Chem Solids 2000;61:1153–7.
[7] Quinn Bernadette M, Lemay Serge G. Single-walled carbon nanotubes as templates and interconnects for nanoelectrodes. Adv Mater 2006;18:855–9.
[8] Popov Valentin N. Carbon nanotubes: properties and application. Mater Sci Eng R 2004;43:61–102.
[9] Kong J, Franklin NR, Zhou C, Chapline MG, Peng S, Cho K, Dai H. Nanotube molecular wires as chemical sensors. Science 2000;287:622–5.
[10] Varghese OK, Kichambre PD, Gong D, Ong KG, Dickey EC, Grimes CA. Gas sensing characteristics of multi-walled carbon nanotubes. Sens Actuat B 2001;81:32–41.
[11] Ghosh S, Sood AK, Kumar N. Carbon nanotube flow sensors. Science 2003;299:1042–4.
[12] Gogotsi Y, Naguib N, Libera JA. In situ chemical experiments in carbon nanotubes. Chem Phys Lett 2002;365:354–60.
[13] Kotsalis EM, Walther JH, Koumoutsakos P. Multiphase water flow inside carbon nanotubes. Int J Multiphase Flow 2004;30:995.
[14] Yoon J, Ru CQ, Mioduchowski A. Vibration and instability of carbon nanotubes conveying fluid. Compos Sci Technol 2005;65:1326–36.
[15] Natsuki T, Ni QQ, Endo M. Wave propagation in single- and double-walled carbon nanotubes filled with fluids. J Appl Phys 2007;101:034319.
[16] Reddy CD, Lu C, Rajendran S, Liew KM. Free vibration analysis of fluid-conveying single-walled carbon nanotubes. Appl Phys Lett 2007;90:133122.
[17] Lu P, Lee HP, Lu C, Zhang PQ. Dynamic properties of flexural beams using a nonlocal elasticity model. J Appl Phys 2006;99:073510.
[18] Wang Q, Varadan VK. Vibration of carbon nanotubes studied using nonlocal continuum mechanics. Smart Mater Struct 2006;15:659–66.
[19] Wang CM, Zhang YY, He XQ. Vibration of nonlocal Timoshenko beams. Nanotechnology 2007;18:105401.
[20] Wang Q, Liew KM. Application of nonlocal continuum mechanics to static analysis of micro- and nano-structures. Phys Lett A 2007;363:236–42.
[21] John P, Shima PD. Thermal properties of nanofluids. Adv Colloid Interface Sci 2012;183–184:30–45.
[22] Daungthongsuk W, Wongwises S. A critical review of convective heat transfer of nanofluids. Renew Sustain Energy Rev 2007;11:797–817.
[23] Huminic G, Huminic A. Application of nanofluids in heat exchangers: a review. Renew Sustain Energy Rev 2012;16(8):5625–38.
[24] Mahian O, Kianifar A, Kalogirou SA, Pop I, Wongwises S. A review of the applications of nanofluids in solar energy. Int J Heat Mass Transfer 2013;57:582–94.
[25] Colangelo G, Favale E, de Risi A, Laforgia D. A new solution for reduced sedimentation flat panel solar thermal collector using nanofluids. Appl Energy 2013;111:80–93.
[26] Xie H, Lee H, Youn W, Choi M. Nanofluids containing multiwalled carbon nanotubes and their enhanced thermal conductivities. J Appl Phys 2003;94:4967–71.
[27] Liu MS, Lin MC, Huang IT, Wang CC. Enhancement of thermal conductivity with carbon nanotube for nanofluids. Int Commun Heat Mass Transfer 2005;32:1202–10.
[28] Maré T, Halelfadl S, Sow O, Estellé P, Duret S, Bazantay F. Comparison of the thermal performances of two nanofluids at low temperature in a plate heat exchanger. Exp Thermal Fluid Sci 2011;35(8):1535–43.
[29] Lalwani Gaurav, Kwaczala Andrea Trinward, Kanakia Shruti, Patel Sunny C, Judex Stefan, Sitharaman Balaji. Fabrication and characterization of three-dimensional macroscopic all-carbon scaffolds. Carbon 2013;53:90–100.
[30] Nield DA, Kuznetsov AV. The Cheng-Minkowycz problem for natural convective boundary-layer flow in a porous medium saturated by a nanofluid. Int J Heat Mass Transfer 2009;52:5792–5.
[31] Kuznetsov AV, Nield DA. Natural convective boundary-layer flow of a nanofluid past a vertical plate. Int J Therm Sci 2010;49:243–7.
[32] Khan WA, Pop I. Boundary-layer flow of a nanofluid past a stretching sheet. Int J Heat Mass Transfer 2010;53:2477–83.
[33] Makinde OD, Aziz A. Boundary layer flow of a nanofluid past a stretching sheet with a convective boundary conditions. Int J Therm Sci 2011;50:1326–32.
[34] Nadeem S, Lee C. Boundary layer flow of nanofluid over an exponentially stretching surface. Nanoscale Res Lett 2012;94(7):1.
[35] Khan W, Khan Z, Rahi M. Fluid flow and heat transfer of carbon nanotubes along a flat plate with Navier slip boundary. Appl Nanosci 2014;4(5):633–41.
[36] Desalination and Water Treatment (PDF). Department of Mechanical Engineering, Massachusetts Institute of Technology; April 2010 [retrieved 17 October 2010].
[37] Thermal conductivity of seawater and its concentrates; 2010. [retrieved 17 October 2010].
[38] World Ocean Atlas 2009. NOAA; 2012 [retrieved 5 December 2012].
[39] Gale, Thomson. Ocean chemical processes; 2006 [retrieved December 2, 2006].
[40] Imtani Ali Nasir. Thermal conductivity for single-walled carbon nanotubes from Einstein relation in molecular dynamics. J Phys Chem Solids 2013;74:1599–603.
[41] Haq Rizwan UI, Nadeem Sohail, Khan ZH, Noor NFM. Convective heat transfer in MHD slip flow over a stretching surface in the presence of carbon nanotubes. Physica B 2015;457:40–7.
[42] Kandasamy R, Muhaimin I, Rosmila AK. The performance evaluation of unsteady MHD non-Darcy nanofluid flow over a porous wedge due to renewable (solar) energy. Renew Energy 2014;64:1–9.
[43] Sattar MA. Unsteady hydromagnetic free convection flow with Hall current, mass transfer and variable suction through a porous medium near an infinite vertical porous plate with constant heat flux. Int J Energy Res 1994;18:771–7.

[44] Kafoussias NG, Nanousis ND. Magnetohydrodynamic laminar boundary layer flow over wedge with suction or injection. Can J Phys 1997;75:733–81.
[45] Murthy PVSN, Mukherjee S, Srinivasacharya D, Krishna PVSSSR. Combined radiation and mixed convection from a vertical wall with suction/injection in a non-Darcy porous medium. Acta Mech 2004;168:145–56.
[46] Schlichting H. Boundary layer theory. New York: McGraw Hill Inc.; 1979.
[47] Talley LD, Pickard GL, Emery WJ, Swift JH. Physical properties of sea water. In: Descriptive physical oceanography. Elsevier Ltd.; 2011. p. 26–65, ISBN: 978-0-7506-4552-2 [chapter 3].

Please cite this article in press as: Kandasamy R et al., Thermal radiation energy due to SWCNTs on MHD nanofluid flow in the presence of seawater/water: Lie group transformation, Ain Shams Eng J (2016), http://dx.doi.org/10.1016/j.asej.2016.04.022